Multi-Scale Block-based Color Constancy

Oguzhan Ulucan, Diclehan Ulucan, Marc Ebner
Institut für Mathematik und Informatik, Universität Greifswald, Greifswald, Germany
{oguzhan.ulucan, diclehan.karakaya, marc.ebner}@uni-greifswald.de

***Abstract*—Removing the effects of the light source from a color-casted image is a key step for numerous computer vision applications. Alongside introducing new color constancy algorithms, researchers also aim at improving the existing methods by utilizing different approaches. Using strategies that have not been investigated in the field of color constancy in detail might help us both to design cost-efficient simple yet effective algorithms and to improve the existing methods. Thereupon, we propose a color constancy method relying on surface orientations which utilizes block-based operations in scale space by only considering the salient regions of the image. According to the evaluations, our multi-scale color constancy method achieves state-of-the-art performance. Moreover, we demonstrate that the performance of several existing color constancy algorithms can be improved by benefiting from scale space.**

***Index Terms*—Computational color constancy, Illumination estimation, Scale space**

I. Introduction

Colors are important cues to understand our surroundings [1]. While the ability to process colors is vital for the survival of many species, it is an essential feature for computer vision systems to carry out several tasks, i.e. object classification and image dehazing. Color processing might be significant for both biological and artificial systems but there is a difference in the way it is performed. Biological systems estimate the reflectance of objects unconsciously by *discounting* the illuminant which is known as *color constancy*, whereas artificial systems have difficulties in carrying out this task. The field of enabling computer vision systems to discount the illuminant and obtain the (shaded) reflectance of the scene is called computational color constancy [2].

We can formulate an image with spatially varying illumination captured by a digital camera as follows;

$$I_i(x, y) = \int R(x, y, \lambda) L(x, y, \lambda) S_i(\lambda) d\lambda \tag{1}$$

where, I_i denotes an image element at a spatial location (x, y), R presents the surface reflectance, L is the wavelength distribution of the light source, S_i is the response function of the color sensor of the capturing device with $i \in \{\text{red, green, blue}\}$, and λ is the wavelength of the visible spectrum.

The aim of color constancy is to remove the color cast caused by the light source L and obtain a canonical image. Since both L and S are unknown, color constancy is an ill-posed problem. Many studies make assumptions to simplify this under-constrained problem by assuming that the light source is uniform at every spatial location in the image and the responses of the color sensors are narrow-band [2]. With these assumptions, the image can be formed as the element-wise product of the surface reflectance R and the global light source L (Eqn. 2).

$$I(x, y) = R(x, y) \cdot L. \tag{2}$$

Numerous color constancy algorithms have been proposed over the years, which are based on different strategies. These approaches can be simply grouped into two categories, statistical-based and data-dependent algorithms. Several of the statistical-based methods are inspired by the mechanisms of the human visual system, which is not surprising, since in computer vision we are trying to mimic our ability to discount the illuminant. For instance, the widely known algorithms in the field of color constancy are the white-patch Retinex and the gray world algorithm which are based on the analyses of the human visual system. While the white-patch Retinex algorithm computes the estimates of the light source by using the maximum response of each image channel individually, the gray world method utilizes the mean of each channel separately [3], [4]. There exist many other statistical-based approaches and several of them also utilize the assumptions of the white-patch Retinex and the gray world algorithms [5], [6], [7], [8], [9], [10], [11], [12], [13], [14]. These traditional methods usually make use of the image statistics while estimating the illuminant of the scene. On the other hand, data-dependent algorithms utilize large-scale datasets and learn features to discount the illuminant [15], [16], [17], [18], [19]. These data-dependent algorithms generally outperform most of the traditional algorithms on current benchmarks. However, as mentioned in many studies, the performance of learning-based methods has a tendency to decrease when they are trying to estimate the illumination of the images captured by a camera whose specifications are unknown and/or the statistical distribution of the illumination condition is different from their training set [11], [13], [20], [21]. The reason behind this performance decay can be related with the facts that *(i)* current benchmarks are mostly formed with similar capturing devices, *(ii)* different illumination conditions are seldomly considered, and *(iii)* learning-based methods expect their training and test sets to be somehow similar [13], [21].

As aforementioned, there are many algorithms relying on different strategies. Utilizing various approaches that have not been analyzed in the field of color constancy in detail may help us to develop cost-efficient simple yet effective algorithms. Thereupon, in our previous studies, we had explicitly shown the advantage of using patches and the salient pixels in the field of color constancy [12], [13], [14]. In short, we demon-

strated that instead of performing global operations, utilizing local computations increases the performance of methods since performing color constancy in a local space allows us to give more importance to varying surface orientations throughout the scene. Furthermore, based on the key biological finding, i.e. the human visual system might be discounting the illuminant based on the highest luminance patches [22], [23], we showed that using only the brightest pixels can improve the performance of an algorithm [14] which also coincides with previous findings where it is stated that not all pixels are informative in color constancy, and utilizing the proper image elements will increase the performance of the algorithms [11], [12], [24]. In this paper, we benefit from the findings of our previous investigations and introduce a multi-scale block-based color constancy algorithm that utilizes the salient pixels in the scene. We carry out the computations at multiple scales since it is well-known that performing computations in scale space enables us to highlight the low-level features of images, i.e. colors [25], [26], [27]. Furthermore, we show that the effectiveness of color constancy methods can be improved by simply carrying out their computations in scale space. To the best of our knowledge, this is the first study that analyzes the impact of scale space computations in learning-free color constancy algorithms in detail.

Our contributions can be summarized as follows:

- We present a simple yet effective learning-free color constancy algorithm that relies on surface orientations by using block-based computations in scale space.
- We demonstrate that the performance of several traditional color constancy algorithms can be improved by carrying out their computations at multiple scales.

This paper is organized as follows. In Sec. II we detail the proposed approach. In Sec. III we demonstrate the performance of our algorithm by comparing it with the state-of-the-art. In Sec. IV we conclude our paper with a brief summary.

II. Proposed Method

We introduce a multi-scale computational color constancy method that benefits from local orientations and the salient pixels in the scene. Our algorithm relies on two assumptions; *(i)* there is at least one bright pixel in the scene, and *(ii)* the world is gray on average.

Our algorithm takes in both sRGB and linear-raw images. In case an sRGB image is given as input, gamma correction is applied to obtain a linear relationship between the image elements. Also, since the saturated pixels may cause noise while estimating the illuminant, we do not consider the darkest and brightest pixels in our computations.

In the field of color constancy, it is known that not every pixel is informative, i.e. dominant sky regions will bias the estimations. Thus, during our computations, we determine the estimates of the light source from the salient regions of the image which contain only the informative pixels. To determine the salient pixels, we convert the image into opponent space as follows [2];

$$\begin{bmatrix} O_{RG} \\ O_{BY} \\ O_{BW} \end{bmatrix} = \begin{pmatrix} \frac{1}{\sqrt{2}} & -\frac{1}{\sqrt{2}} & 0 \\ \frac{1}{\sqrt{6}} & \frac{1}{\sqrt{6}} & -\frac{\sqrt{2}}{\sqrt{3}} \\ \frac{1}{\sqrt{3}} & \frac{1}{\sqrt{3}} & \frac{1}{\sqrt{3}} \end{pmatrix} \begin{bmatrix} R \\ G \\ B \end{bmatrix} \tag{3}$$

where, O_{RG}, O_{BY}, and O_{BW} are the red-green, blue-yellow, and black-white opponent channels, respectively.

Since the human visual system might be discounting the illuminant based on the highest luminance in the scene, we take the top 3.8% brightest pixels in the black-white opponent channel, i.e. brightness, of the image to form a binary saliency map $\mathcal{S}$, where the informative pixels are highlighted (the analysis of this parameter is provided in Sec. III).

Since the pixels highlighted by the saliency map do not have an equal contribution, alongside the saliency map, we adaptively form a weight map $\mathcal{W}$ from the black-white opponent channel O_{BW} of the image at each spatial location using a Gaussian curve (Eqn. 4). This weight map gives more importance to the brightest pixels while reducing the contribution of the darkest pixels.

$$\mathcal{W}(x,y) = 1 - \frac{1}{2\pi\sigma^2} exp\left(-\frac{(O_{BW}(x,y)-\mu)^2}{2\sigma^2}\right) \tag{4}$$

where, μ and σ are the mean and the standard deviation of O_{BW}, respectively. We normalized $\mathcal{W}$ so that the summation of its elements equals to 1.

After we extract the saliency and weight maps, we form an informative image $\mathcal{I}$ as follows;

$$\mathcal{I} = I(x,y) \cdot \mathcal{W}(x,y) \cdot \mathcal{S}(x,y). \tag{5}$$

Then, we downsample the informative image to obtain representations at different scales, where the number of levels $\mathcal{L}$ is determined adaptively and depends on the image resolution. Subsequently, at finer scales the image is divided into non-overlapping blocks containing a certain number of pixels m, where m is determined adaptively according to the corresponding image resolution at the scale as follows;

$$m = \sqrt{(h \cdot w)/\eta} \tag{6}$$

where, h and w are the height and width of the image, and η is the controlling parameter of m, which is determined practically as 120 (the investigation of this parameter is given in Sec. III). Note here that at the coarser scales, the number of pixels falling into a block will be insufficient to validate the assumptions of our algorithm, i.e. the world is gray on average since the gray world algorithm is only valid when there is an adequate number of different colors is available in the scene [2]. Therefore, we experimentally determined that dividing the image into blocks will be inefficient at scales higher than half of the number of possible levels that can be reached.

Afterwards, at every scale we find the descriptors to compute the illuminant either in each block in the case of finer scales or in each image in the case of coarser scales. Since our algorithm relies on the assumptions of the white-patch Retinex and gray world method, we assume that for each patch P (or image at coarser scales, which henceforth will be referred to also as P for simplicity) there exists at least one bright pixel and a unique gray value, which are the descriptors to estimate the illuminant. Firstly, for each P we determine the brightest pixels by taking the maximum response of each channel individually. Subsequently, we form a vector $\mathbf{P}_{max} = [P_{r,max}, P_{g,max}, P_{b,max}]$, which is our first descriptor. Secondly, we calculate the gray value P_μ for each P by taking the mean over all channels within the region of interest, which is our second descriptor. One can argue that the gray value can be found by directly taking the mean of all pixels in the image but we observed that using the same gray value for all patches decreases the performance of the algorithm. This performance decay is not surprising if we consider the fact that the local surface orientations of the scene differ throughout the image, i.e. there exists a unique gray value for each block.

After we obtain both descriptors, we compute the estimate of the illuminant of each patch by taking our second assumption, i.e. the world is gray on average, into account. We assume that if the scene is gray on average then the summation of the intensity values of $\mathbf{P}_{max}$ should be gray. However, there will be a shift away from the gray world in case there is a color cast in the scene. Thereupon, for each P we determine this deviation by computing a scaling vector $\mathbf{C}_P = [c_r, c_g, c_b]$. $\mathbf{C}_P$ scales the intensities of the $\mathbf{P}_{max}$ such that they sum to a gray value P_μ as follows;

$$P_{r,max} \cdot c_r + P_{g,max} \cdot c_g + P_{b,max} \cdot c_b = P_\mu. \tag{7}$$

This scaling vector $\mathbf{C}_P$ can be calculated by solving the following optimization problem;

$$\mathbf{C}_P = \arg\min_{\mathbf{C}_P} \left\| P_{max}\ \mathbf{C}_P - P_\mu \right\|_2 \ \ with\ \forall c \in \mathbf{C}_P\ :\ c \geq 0. \tag{8}$$

In order to find a single estimate for each scale we average the computed $\mathbf{C}_P$ as follows;

$$\hat{\mathbf{L}}_s = \frac{1}{n} \sum_{k=1}^{n} \mathbf{C}_{P_k} \tag{9}$$

where, $\hat{\mathbf{L}}_s$ is an illuminant estimate at a particular scale s with $s \in \mathcal{L}$, and n is the number of blocks.

In order to find the color vector of the global light source $\hat{\mathbf{L}}_{est}$, we linearly combine the estimates of different scales as follows;

$$\hat{\mathbf{L}}_{est} = \frac{1}{\mathcal{L}} \sum_{s=1}^{\mathcal{L}} \hat{\mathbf{L}}_s. \tag{10}$$

Lastly, the canonical image can be obtained by scaling the color casted image according to $\hat{\mathbf{L}}_{est}$ by using Eqn. 2.

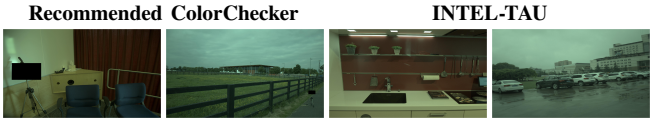

Fig. 1: Example indoor and outdoor scenes from benchmarks. Gamma correction is applied for better visualization.

III. Experimental Results and Discussion

We investigated the performance of the proposed method and the effectiveness of carrying out the computations of several color constancy algorithms into scale space by comparing them with the following learning-based color constancy algorithms; Quasi-Unsupervised CC [15], C3AE [16], SIIE [17], FFCC [18], C5 [19], and with the following learning-free color constancy algorithms; maxRGB [3], GW [4], SoG [5], 1^{st} order GE [6], WGE [7], DOCC [9], PCA-CC [8], MSGP [10], GI [11], BB-CC [13], BIO-CC [12]. While all learning-free algorithms whose codes are available are utilized without any optimization, the results of the remaining algorithms are reported based on the publications of these works.

We evaluated the algorithms on two color constancy benchmarks, namely, Recommended ColorChecker [28] and INTEL-TAU [29] datasets (Fig. 1). The Recommended ColorChecker dataset consists of a total of 568 images captured by two different cameras, Canon 1D and Canon 5D, while the INTEL-TAU dataset contains a total of 7022 scenes captured with three different devices, Mobile Sony IMX135, Nikon D810, and Canon 5DSR. All the images in both datasets have a linear response and their black level is calibrated. It is important to note here that some of the images in the INTEL-TAU dataset contain color charts and since their masks are not provided, we did not consider these images in our experiments. Also, for both benchmarks, we combined the images which are captured with different cameras to create a single set since it is important to evaluate the algorithms with images whose spectral distributions are unknown [11], [12].

To obtain statistical results, we computed the angular error ε between the ground truth illuminant $\mathbf{L}_{gt}$ and the estimated illuminant $\hat{\mathbf{L}}_{est}$ (Eqn. 11). We report the mean, the median, the mean of the best 25%, and the mean of the worst 25% of the angular error in Table I.

$$\varepsilon(\mathbf{L}_{gt}, \hat{\mathbf{L}}_{est}) = cos^{-1}\left(\frac{\mathbf{L}_{gt}\hat{\mathbf{L}}_{est}}{\|\mathbf{L}_{gt}\|\|\hat{\mathbf{L}}_{est}\|} \right). \tag{11}$$

While investigating the performance of our approach, first we analyzed how the extracted weights and the saliency map affects the performance of the proposed method. As we can see from Table I, when we estimate the color vector of the light source by only considering image elements with the highest luminance while also weighting the input image according to the contribution of the brightest pixels, the performance of the algorithm improves significantly. The errors of both the best and the worst cases decrease, thus the mean angular error reduces substantially.

TABLE I: Statistical results. Top three results are highlighted.

	Algorithms	RECommended ColorChecker Mean	Median	Best 25%	Worst 25%	INTEL-TAU Mean	Median	Best 25%	Worst 25%
Learning	Quasi-Unsupervised CC	3.46	2.23	-	-	**3.12**	**2.19**	0.60	**7.28**
	C3AE	**2.10**	**1.90**	0.80	**4.00**	3.40	2.70	0.90	**7.00**
	SIIE	**2.77**	**1.93**	0.55	**6.53**	3.42	2.42	0.73	7.80
	FFCC	2.95	2.19	0.57	6.75	3.42	2.38	0.70	7.96
	C5	**2.50**	**1.99**	0.53	**5.46**	**2.52**	**1.70**	**0.52**	**5.96**
Traditional	maxRGB	10.27	9.12	1.64	20.50	11.01	13.16	1.81	19.45
	GW	4.74	3.61	0.97	10.44	4.91	3.88	0.96	10.60
	SoG	5.87	4.25	0.75	13.72	5.51	4.16	0.97	12.29
	1^{st} GE	6.42	3.84	0.94	15.84	6.10	4.23	0.96	14.27
	WGE	6.10	3.33	0.80	15.59	6.00	3.64	0.81	14.90
	DOCC	7.24	4.26	0.80	18.05	7.19	4.67	0.81	16.98
	PCA-CC	4.11	2.52	0.53	10.19	4.47	3.03	0.69	10.64
	MSGP	3.81	2.96	0.77	8.35	3.57	2.57	0.64	8.24
	GI	3.20	**1.90**	**0.44**	8.02	3.33	**2.18**	**0.56**	8.03
	BB-CC	3.82	3.17	1.46	7.38	4.30	3.61	1.20	8.53
	BIO:CC	4.40	3.30	0.86	9.85	4.15	3.06	0.76	9.42
Multi-scale	maxRGB	3.82	2.58	0.84	8.85	3.77	2.87	0.92	8.15
	GW	4.13	3.02	0.67	9.45	4.51	3.49	0.81	9.87
	SoG	3.66	2.32	**0.49**	9.17	4.01	2.95	0.71	9.10
	1^{st} GE	3.52	2.19	**0.49**	8.74	3.87	2.80	0.71	8.87
	DOCC	3.56	2.29	**0.49**	8.75	3.55	2.62	0.64	8.06
	PCA-CC	3.67	2.29	**0.47**	9.22	3.98	2.82	0.63	9.35
	Proposed without $\mathcal{W}$ and $\mathcal{S}$	3.69	2.86	0.84	7.97	3.98	3.06	0.84	8.65
	Proposed	3.18	2.21	0.61	7.36	**3.23**	2.23	**0.59**	7.48

Our method achieves the best mean and the worst 25% of the angular error among the learning-free methods on both datasets while it produces competitive scores compared to the learning-based models. Also, our algorithm's median angular error is significantly less than its mean angular error, which indicates that our method tends to produce outcomes closer to the best cases rather than the worst ones. The statistical outcomes are also coinciding with the visual comparisons in Fig 2. For both indoor and outdoor scenes, the proposed method estimates the color vector of the light source accurately. However, when the uniformity of the color distribution of the scene increases throughout the image, the efficiency of the algorithm decreases (Fig 2). This is also a well-known problem among traditional color constancy algorithms.

Moreover, we provide a brief investigation about the analysis of the effectiveness of using multiple scales by carrying out the computations of different color constancy algorithms in scale space. It is important to stress that before applying the algorithms in scale space, we remove the saturated pixels from the input image to eliminate possible noise since we observed that these pixels negatively affect the outcomes of the algorithms. Afterwards, we apply the methods at each scale to estimate the color vector of the illumination. Then, we average over all scales to find the estimate of the global light source. Consequently, the performance of the existing algorithms increases significantly in terms of all metrics (Table I). They outperform their original versions, while they produce competitive results by outperforming several other color constancy algorithms on both datasets. Furthermore, it is known that while reducing the mean angular error as much as possible, it is also important to improve the mean of the worst 25% of the angular error of the algorithms [12], [13]. A noteworthy outcome of carrying the computations into scale space is that it allows the color constancy approaches to improve their worst cases on both benchmarks (Fig 3). Also, in

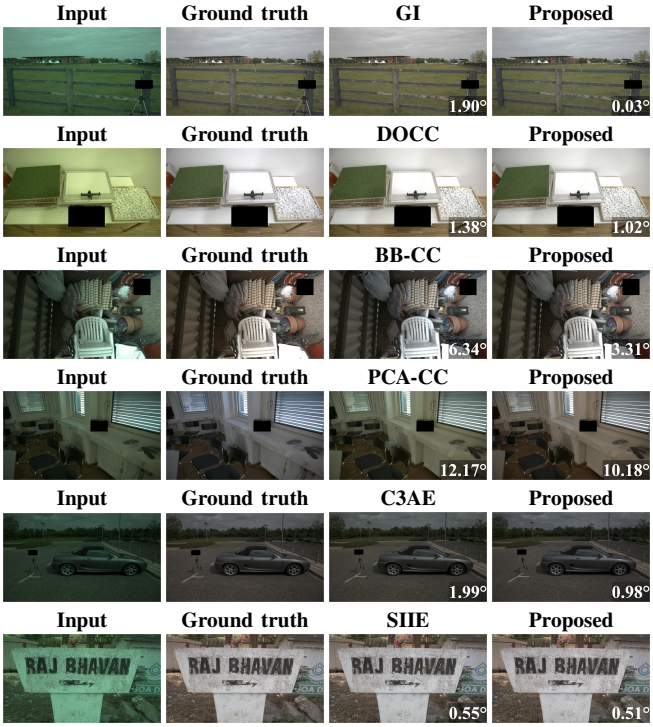

Fig. 2: Visual comparison of the proposed method with different color constancy algorithms on random indoor and outdoor scenes. The angular error is provided on the bottom-right side of the image.

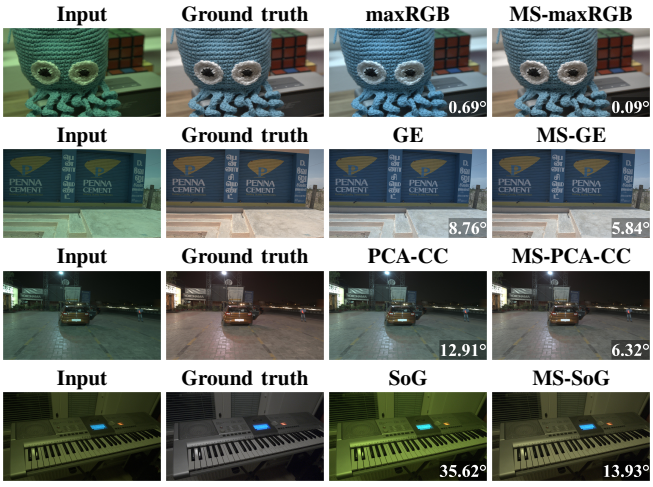

Fig. 3: Visual comparisons of the algorithms with their multi-scale (MS) versions. The angular error is provided on the bottom-right side of the image.

terms of the mean of the best 25% of the angular error, the best scores among all methods are obtained when the algorithms are applied in scale space.

Lastly, we provide a brief discussion about how we determine the parameters of our method. While the number of pixels falling into non-overlapping blocks is highly dependent

TABLE II: Parameter selection. Best combination is chosen.

Controlling parameter η	The top % of brightest pixels									
	3%	**3.2**%	**3.4**%	**3.6**%	**3.8**%	**4**%	**4.2**%	**4.4**%	**4.6**%	**4.8**%
20	3.47	3.45	3.45	3.46	3.45	3.49	3.49	3.50	3.51	3.52
40	3.49	3.48	3.47	3.48	3.48	3.49	3.48	3.48	3.48	3.49
60	3.44	3.43	3.43	3.42	3.42	3.45	3.46	3.46	3.48	3.49
80	3.43	3.42	3.43	3.44	3.44	3.46	3.45	3.46	3.47	3.48
100	3.47	3.45	3.45	3.45	3.44	3.46	3.47	3.48	3.49	3.50
120	3.39	3.37	3.37	3.37	**3.36**	3.38	3.40	3.42	3.43	3.43
140	3.43	3.42	3.41	3.42	3.42	3.43	3.43	3.44	3.45	3.47
160	3.45	3.44	3.43	3.43	3.43	3.44	3.441	3.44	3.45	3.46
180	3.43	3.41	3.40	3.40	3.40	3.41	3.42	3.43	3.44	3.45
200	3.46	3.45	3.45	3.43	3.43	3.44	3.45	3.47	3.48	3.49

on the image resolution, the top brightest pixels that we consider to form our saliency map are associated with image statistics. We determine these parameters based on the mean angular error on a subset which is created by randomly choosing images from both datasets. As seen in Table II, when a patch contains an adequate number of pixels the effectiveness of the proposed method increases. This can be explained by two facts; *(i)* when the size of the blocks is sufficient, the possibility of having uniform colored regions decreases, hence the assumption of the gray world is validated, and *(ii)* the surface orientations are varying throughout the image, thus when we consider sufficiently large local regions, the chance of taking local surface orientations into account increases. Also, the performance of our algorithm is affected by the number of the brightest pixels used to form the saliency map. After investigating the responses of the algorithm, we selected the top 3.8% of the brightest pixels.

IV. Conclusion

Color constancy has a significant role in many applications. Due to its importance, computational color constancy is widely studied, and over decades many successful algorithms are introduced. Alongside developing new algorithms, researchers also aim at improving existing methods since combining different strategies might help us to design cost-efficient simple yet effective algorithms. Thereupon, by making use of our previous investigations we propose an algorithm that relies on block-based operations carried out in multiple scales by only considering the salient regions of the scenes. According to the experiments, our method achieves competitive results on two different benchmarks while outperforming several of the learning-based methods. Also, we show that the efficiency of several color constancy algorithms can be improved by simply carrying out their computations in scale space. As future work, we will modify our algorithm for mixed illumination conditions and provide more investigations on global color constancy.

References

[1] S. Zeki, *A Vision of the Brain*, Blackwell Science, 1993.

[2] M. Ebner, *Color Constancy, 1st ed.*, Wiley Publishing, 2007.

[3] E. H. Land, "The retinex theory of color vision," *Scientific Amer.*, vol. 237, pp. 108–129, 1977.

[4] G. Buchsbaum, "A spatial processor model for object colour perception," *J. Franklin Inst.*, vol. 310, pp. 1–26, 1980.

[5] G. D. Finlayson and E. Trezzi, "Shades of gray and colour constancy," in *Color and Imag. Conf.* Society for Imaging Science and Technology, 2004, pp. 37–41.

[6] J. Van De Weijer, T. Gevers, and A. Gijsenij, "Edge-based color constancy," *IEEE Trans. Image Process.*, vol. 16, pp. 2207–2214, 2007.

[7] A. Gijsenij, T. Gevers, and J. Van De Weijer, "Physics-based edge evaluation for improved color constancy," in *Conf. Comput. Vision Pattern Recognit.* IEEE, 2009, pp. 581–588.

[8] D. Cheng, D. K. Prasad, and M. S. Brown, "Illuminant estimation for color constancy: Why spatial-domain methods work and the role of the color distribution," *J. Opt. Soc. America A*, vol. 31, pp. 1049–1058, 2014.

[9] S.-B. Gao, K.-F. Yang, C.-Y. Li, and Y.-J. Li, "Color constancy using double-opponency," *IEEE Trans. Pattern Anal. Mach. Intell.*, vol. 37, no. 10, pp. 1973–1985, 2015.

[10] Y. Qian, S. Pertuz, J. Nikkanen, J.-K Kämäräinen, and J. Matas, "Revisiting gray pixel for statistical illumination estimation," *arXiv preprint arXiv:1803.08326*, 2018.

[11] Y. Qian, J.-K. Kamarainen, J. Nikkanen, and J. Matas, "On finding gray pixels," in *Conf. Comput. Vision Pattern Recognit.* IEEE/CVF, 2019, pp. 8062–8070.

[12] O. Ulucan, D. Ulucan, and M. Ebner, "BIO-CC: Biologically inspired color constancy," in *Brit. Mach. Vision Conf.* BMVA Press, 2022.

[13] O. Ulucan, D. Ulucan, and M. Ebner, "Color constancy beyond standard illuminants," in *Int. Conf. Image Process.* IEEE, 2022, pp. 2826–2830.

[14] O. Ulucan, D. Ulucan, and M. Ebner, "Block-based color constancy: The deviation of salient pixels," in *Int. Conf. Acoust. Speech Signal Process.* IEEE, 2023, pp. 1–5.

[15] S. Bianco and C. Cusano, "Quasi-unsupervised color constancy," in *Conf. Comput. Vision Pattern Recognit.* IEEE/CVF, 2019, pp. 12212–12221.

[16] F. Laakom, J. Raitoharju, A. Iosifidis, J. Nikkanen, and M. Gabbouj, "Color constancy convolutional autoencoder," in *Symp. Ser. Comput. Intell.* IEEE, 2019, pp. 1085–1090.

[17] M. Afifi and M. S. Brown, "Sensor-independent illumination estimation for DNN models," *Brit. Mach. Vision Conf.*, 2019.

[18] J. T. Barron and Y. T. Tsai, "Fast fourier color constancy," in *Conf. Comput. Vision Pattern Recognit.* IEEE/CVF, 2017, pp. 886–894.

[19] M. Afifi, J. T. Barron, C. LeGendre, Y.-T. Tsai, and F. Bleibel, "Cross-camera convolutional color constancy," in *Int. Conf. Comput. Vision*. IEEE/CVF, 2021, pp. 1981–1990.

[20] S. Gao, M. Zhang, C. Li, and Y. Li, "Improving color constancy by discounting the variation of camera spectral sensitivity," *J. Opt. Soc. America A*, vol. 34, pp. 1448–1462, 2017.

[21] M. Buzzelli, S. Zini, S. Bianco, G. Ciocca, R. Schettini, and M. K. Tchobanou, "Analysis of biases in automatic white balance datasets and methods," *Color Res. Appl.*, vol. 48, no. 1, pp. 40–62, 2023.

[22] D.H. Foster and K.J. Linnell, "Space-average scene colour used to extract illuminant information," in *John Dalton's Colour Vision Legacy: Dickinson, I. Murray, & D. Carden*, pp. 201–209. Taylor & Francis, 1997.

[23] M. Ebner, "A parallel algorithm for color constancy," *J. Parallel Distrib. Comput.*, vol. 64, pp. 79–88, 2004.

[24] T. Ono, Y. Kondo, L. Sun, T. Kurita, and Y. Moriuchi, "Degree-of-linear-polarization-based color constancy," in *Conf. Comput. Vision Pattern Recognit.* IEEE/CVF, 2022, pp. 19740–19749.

[25] B. Li, D. Xu, M. H. Lee, and S.-H. Feng, "A multi-scale adaptive grey world algorithm," *Trans. Inf. Syst.*, vol. 90, no. 7, pp. 1121–1124, 2007.

[26] D. Ulucan, O. Ulucan, and M. Ebner, "Multi-scale surface normal estimation from depth maps," in *Int. Conf. Image Process. Vision Eng.* INSTICC, 2023, pp. 47–56.

[27] D. Ulucan, O. Ulucan, and M. Ebner, "Intrinsic image decomposition: Challenges and new perspectives," in *Int. Conf. Image Process. Vision Eng.* INSTICC, 2023, pp. 57–64.

[28] G. Hemrit, G. D. Finlayson, A. Gijsenij, P. Gehler, S. Bianco, B. Funt, M. Drew, and L. Shi, "Rehabilitating the colorchecker dataset for illuminant estimation," in *Color Imag. Conf.* Society for Imaging Science and Technology, 2018, pp. 350–353.

[29] F. Laakom, J. Raitoharju, J. Nikkanen, A. Iosifidis, and M. Gabbouj, "INTEL-TAU: A color constancy dataset," *IEEE Access*, vol. 9, pp. 39560–39567, 2021.